

Energetic stability of coreless vortices in spin-1 Bose-Einstein condensates with conserved magnetization

Justin Lovegrove, Magnus O. Borgh, and Janne Ruostekoski
School of Mathematics, University of Southampton, SO17 1BJ, Southampton, UK
(Dated: November 9, 2018)

We show that conservation of longitudinal magnetization in a spinor condensate provides a stabilizing mechanism for a coreless vortex phase-imprinted on a polar condensate. The stable vortex can form a composite topological defect with distinct small- and large-distance topology: the inner ferromagnetic coreless vortex continuously deforms toward an outer singular, singly quantized polar vortex. A similar mechanism can also stabilize a nonsingular nematic texture in the polar phase. A weak magnetization is shown to destabilize a coreless vortex in the ferromagnetic phase.

PACS numbers: 03.75.Lm, 03.75.Mn, 67.85.Fg, 11.27.+d,

In ordinary superfluids, quantization of circulation around a singular core is a hallmark of superfluidity. In superfluids with internal degrees of freedom, circulation need not be quantized, and it becomes possible for angular momentum to be carried by nonsingular textures. The canonical examples are the Anderson-Toulouse-Chechetkin (ATC) [1, 2] and Mermin-Ho (MH) [3] vortices in superfluid liquid ^3He . Coreless spin textures are also well known in quantum Hall physics [4].

An optically trapped atomic spin-1 Bose-Einstein condensate (BEC) exhibits two phases of the ground-state manifold. Coreless vortices naturally occur in the ferromagnetic (FM) phase, where the order parameter is determined by spatial spin rotations and circulation alone is not quantized [5, 6]. Angular momentum is then carried by a characteristic, nonsingular fountainlike spin texture [7–11]. In the polar phase, by contrast, the expectation value of the spin vanishes, vortices are singular, and circulation is quantized [5, 6].

Experiments, however, have demonstrated that the longitudinal magnetization of the condensate is approximately conserved on the time scales of current alkali-metal atom experiments [12–14] and its value can be controlled. In strongly magnetized BECs, coreless vortices have indeed been prepared by phase-imprinting in the polar interaction regime [15–17] where nonsingular vortices would not be expected to appear by simple energetic arguments alone.

Here we study coreless, nonsingular vortex textures of spin-1 BECs in the general case where the system is no longer confined to either the FM or polar ground-state manifold. We construct analytic models of their spinor wave functions that interpolate between the two manifolds. The energetic stability of imprinted coreless textures is analyzed when the longitudinal magnetization is strictly constrained throughout the energy-relaxation process. We show that the coreless vortex, formed by the spin texture, can be energetically stable in the polar regime for sufficiently strong magnetization. In the stable configuration, the magnetization leads to a mixing of the polar and FM phases with a hierarchical core struc-

ture: The interior core region $\rho = (x^2 + y^2)^{1/2} \lesssim \eta_M$, where η_M is the characteristic length scale determined by the magnetization constraint, exhibits a coreless vortex analogous to the coreless vortex in the FM phase. In the outer region, $\rho \gtrsim \eta_M$, the coreless vortex continuously deforms toward a singly quantized, singular polar vortex. With distinct small- and large-distance topology, the vortex represents a *composite topological defect*. Composite vortices also exist in superfluid liquid ^3He , in which case the hierarchy of different core structures can result from different interaction energies, owing, e.g., to spin-orbit or magnetic-field coupling [18, 19].

The vortex core can also be understood in terms of characteristic energetic length scales. In a spin-1 BEC, where the magnetization is not conserved, the core size is determined by the larger of the two healing lengths ξ_F or ξ_n [20–22]. These describe, respectively, the distance over which local perturbations of the spin expectation value or the density heal. When the conserved magnetization yields $\eta_M \gtrsim \max(\xi_F, \xi_n)$, it becomes energetically favorable to form a core of size η_M , with sharply varying magnetization density.

The phase-imprinting technique employed to create the coreless vortex with the fountainlike spin texture in Refs. [15, 16] can also be used to prepare a *nematic coreless vortex* [16, 17] in the polar regime, in which case the characteristic texture is formed by the nematic axis. The nematic coreless vortex does not carry angular momentum, and therefore cannot be stabilized by rotation. We show that a sufficiently strong magnetization, however, can energetically stabilize the nematic coreless vortex. This happens when the magnetization is strong enough to empty one of the spinor components and form an effective two-component system. The stable configuration may also be understood in terms of a composite vortex: in the inner region the nematic axis forms a fountainlike coreless texture that continuously deforms in the outer region to a singular, singly quantized FM vortex. The spin profile then provides a constraint, stabilizing the nematic coreless vortex inside the core.

Substantial deviations of the conserved magnetization

from its ‘natural’ value can also affect the FM regime. We show that a singly quantized FM vortex can form the ground state in a rotating condensate. This may seem surprising, since in that case coreless vortices are otherwise predicted to make up the ground state [8–11]. We find that the spin structure of the coreless vortex cannot support a *weak* magnetization and the singly quantized singular vortex, which would normally exhibit higher energy than the coreless vortex [21], becomes the new ground state.

We consider the classical mean-field theory of the spin-1 BEC, with the wave function given by the atom density $n(\mathbf{r})$ and a three-component spinor $\zeta(\mathbf{r})$,

$$\Psi(\mathbf{r}) = \sqrt{n(\mathbf{r})}\zeta(\mathbf{r}) = \sqrt{n(\mathbf{r})} \begin{pmatrix} \zeta_+(\mathbf{r}) \\ \zeta_0(\mathbf{r}) \\ \zeta_-(\mathbf{r}) \end{pmatrix}, \quad \zeta^\dagger \zeta = 1. \quad (1)$$

The s -wave interaction between two spin-1 atoms, with the scattering lengths a_0 and a_2 , acquires a spin-dependent contribution, yielding two interaction terms [$c_0 = 4\pi\hbar^2(2a_2 + a_0)/3m$ and $c_2 = 4\pi\hbar^2(a_2 - a_0)/3m$] in the Hamiltonian density [23],

$$\mathcal{H} = \frac{\hbar^2}{2m} |\nabla\Psi|^2 + \frac{1}{2}m\omega^2 r^2 n + \frac{c_0}{2}n^2 + \frac{c_2}{2}n^2 |\langle \hat{\mathbf{F}} \rangle|^2, \quad (2)$$

where ω is the trap frequency. The spin operator $\hat{\mathbf{F}}$ is defined as a vector of spin-1 Pauli matrices, and its expectation value $\langle \hat{\mathbf{F}} \rangle = \zeta_\alpha^\dagger \hat{\mathbf{F}}_{\alpha\beta} \zeta_\beta$ yields the local spin vector.

The sign of c_2 in Eq. (2) determines which phase is energetically favored by the spin-dependent interaction alone. If $c_2 > 0$, as with ^{23}Na , the polar phase with $|\langle \hat{\mathbf{F}} \rangle| = 0$ is preferred. The order parameter is then defined by a BEC phase ϕ and an unoriented nematic axis $\hat{\mathbf{d}}$ [5, 6], such that $\zeta(\phi, \hat{\mathbf{d}}) = \zeta(\phi + \pi, -\hat{\mathbf{d}})$. The nematic order leads to the existence of vortices with both integer and half-integer [24] winding.

Conversely if $c_2 < 0$, as with ^{87}Rb , the FM phase with $|\langle \hat{\mathbf{F}} \rangle| = 1$ is favored. All FM spinors are related by 3D spin rotations, which define the order parameter space. This supports two classes of line defects [7, 25]. The nontrivial representatives of each class are singular, singly quantized vortices and nonsingular, coreless vortices, respectively.

The rich phenomenology of the spin-1, and higher-spin, order-parameter spaces provides an intriguing system for studies of defects and textures [5, 7–11, 20–22, 24–43]. Experimentally, vortices and spin textures have been investigated by means of both controlled preparation [15–17, 44] and dynamical formation [45–48]. Here we consider the energetic stability of a coreless vortex when the magnetization is conserved. The coreless vortex may be phase-imprinted onto a BEC with initially uniform spin texture, regardless of the sign of c_2 . The imprinted vortex state then relaxes due to energy dissipation and we investigate its structure and stability. The magnetization

constraint may in general force the wave function out of its ground-state manifold by mixing the FM and polar phases. We will show that the energy relaxation of the prepared vortex can then be analyzed by introducing the following spinor wave function

$$\zeta^{\text{cl}}(\mathbf{r}) = \frac{1}{2} \begin{pmatrix} \sqrt{2} \left(f_- \sin^2 \frac{\beta}{2} - f_+ \cos^2 \frac{\beta}{2} \right) \\ -e^{i\varphi} (f_- + f_+) \sin \beta \\ \sqrt{2} e^{2i\varphi} \left(f_- \cos^2 \frac{\beta}{2} - f_+ \sin^2 \frac{\beta}{2} \right) \end{pmatrix}. \quad (3)$$

Here $f_\pm = \sqrt{1 \pm F}$, so that in cylindrical coordinates (ρ, φ, z) the spin vector $\langle \hat{\mathbf{F}} \rangle = F(\sin \beta \hat{\boldsymbol{\rho}} + \cos \beta \hat{\mathbf{z}})$, with $|\langle \hat{\mathbf{F}} \rangle| = F$, displaying the characteristic fountainlike texture. The coreless vortex (3) interpolates between the FM and polar phases with $0 \leq F \leq 1$. It can be constructed from a generalized spinor by combining a 2π winding of the BEC phase with a spin rotation [23].

In the limit $F = 1$, the spinor (3) represents the ordinary coreless vortex solution in the FM phase, with the spin orientation $\beta(\rho)$ increasing monotonically from zero at $\rho = 0$. In the opposite limit $F = 0$, it becomes a singly quantized polar vortex, with $\hat{\mathbf{d}} = \cos \beta \hat{\boldsymbol{\rho}} - \sin \beta \hat{\mathbf{z}}$, displaying a radial disgyration for $\beta \neq \pi/2$ [23]. Now we let F vary in space such that $F(\rho \rightarrow 0) \rightarrow 1$ and $F \rightarrow 0$ for large ρ . Equation (3) then describes a *composite* vortex, where the inner coreless vortex forms the core of the outer polar vortex, and the circulation $\nu = \oint \mathbf{dr} \cdot \mathbf{v} = \frac{\hbar}{m} (1 - F \cos \beta)$ interpolates smoothly between the corresponding regions [23].

The coreless vortex is analogous to the nonsingular ATC [1, 2] and MH [3] textures in superfluid liquid ^3He [23]. For the coreless texture, one may define a winding number similar to that of a point defect,

$$W = \frac{1}{8\pi} \int_{\mathcal{S}} d\Omega_i \epsilon_{ijk} \hat{\mathbf{n}}_F \cdot \left(\frac{\partial \hat{\mathbf{n}}_F}{\partial x_j} \times \frac{\partial \hat{\mathbf{n}}_F}{\partial x_k} \right), \quad (4)$$

where $\hat{\mathbf{n}}_F = \langle \hat{\mathbf{F}} \rangle / |\langle \hat{\mathbf{F}} \rangle|$ and \mathcal{S} denotes the upper hemisphere. The charge W counts the number of times $\langle \hat{\mathbf{F}} \rangle$ wraps around the full order parameter space. If the spin vector reaches a uniform asymptotic orientation everywhere away from the vortex (i.e., the bending angle $\beta(\rho)$ is an integer multiple of π), W represents an integer-valued charge. This charge is conserved whenever the boundary condition is fixed, e.g., by physical interaction or energetics. If no boundary condition is imposed, the texture can unwind to the vortex-free state by purely local transformations of the wave function. The spin-1 coreless vortex may be stabilized by rotation as the bending angle $\beta(\rho)$ in Eq. (3), and therefore the superfluid circulation, adapts to the imposed rotation. As a result of (4), coreless textures are also called 2D ‘baby Skyrmions’ [49] in analogy with the 3D Skyrmions [50], which represent stable particlelike solitons that can also exist in atomic BECs [51–55].

Magnetic-field rotation [56–58] can be used to phase-imprint a coreless vortex [15, 16]. In Ref. [16], the axial bias field B_z of an external magnetic quadrupole field $\mathbf{B} = B'\rho\hat{\rho} + (B_z - 2B'z)\hat{z}$, is swept linearly such that the zero-field point passes through an initially spin-polarized BEC $\zeta^1 = (1, 0, 0)^T$ [59]. The sweep amounts to a spin rotation $\zeta^1 = \exp[-i\hat{\mathbf{F}} \cdot \beta(\rho)\hat{\varphi}]\zeta^1$, resulting in the coreless vortex (3), with $F = 1$ everywhere. A (pseudo)spin-1 coreless vortex has also been phase-imprinted in the $|m = 0, \pm 2\rangle$ levels of a spin-2 ^{87}Rb BEC (with the $|m = \pm 1\rangle$ levels empty) through population transfer using a Laguerre-Gaussian laser [23, 44].

By adjusting the spin orientation $\beta(\rho)$ in imprinting experiments, one can accurately control the longitudinal BEC magnetization $M = (N_+ - N_-)/N$, where N_{\pm} and N are the $|m = \pm 1\rangle$ and total atom numbers, respectively. Owing to the conservation of angular momentum in s -wave scattering, the only spin-flip processes as the energy relaxes are $2|m = 0\rangle \rightleftharpoons |m = +1\rangle + |m = -1\rangle$, which do not change the magnetization. Consequently M is approximately conserved as the imprinted texture relaxes on time scales where s -wave scattering dominates, e.g., over dipolar interactions and collisions with high-temperature atoms [12–14, 60]. Dynamical stability of a cylindrically symmetric magnetized coreless vortex was demonstrated against low-energy, cylindrically symmetric Bogoliubov modes in Ref. [38].

We first study the energetic stability of the phase-imprinted coreless vortex in the polar regime. As an initial state we take the magnetically rotated ζ^1 [Eq. (3) with $F = 1$ everywhere], for different M . The energetic stability and structure of the vortex is then determined by numerically minimizing the free energy in a rotating trap (at the frequency Ω). We take $Nc_0 = 1000\hbar\omega l^3$ and $c_0/c_2 \simeq 28$ of ^{23}Na [61] in Eq. (2), where $l = (\hbar/m\omega)^{1/2}$. We strictly conserve the longitudinal magnetization of the initial state throughout the relaxation procedure. The physical mechanism is therefore different from that used in numerical techniques to achieve a nonzero magnetization for the final state by means of an effective linear Zeeman term, without explicitly conserving the magnetization during relaxation [8, 27–29].

In a spin-1 BEC a vortex singularity can be accommodated by exciting the wave function out of its ground-state manifold, whenever it is energetically more favorable to adjust the spin value than force the density to vanish at the singular core [20, 21]. This happens when the characteristic length scales $\xi_n = l(\hbar\omega/2c_0n)^{1/2}$ and $\xi_F = l(\hbar\omega/2|c_2|n)^{1/2}$ satisfy $\xi_F \gtrsim \xi_n$. Conservation of magnetization introduces a third length scale η_M that describes in the polar phase the size of a FM core needed to yield the required M . By considering a uniformly magnetized cylindrical core inside an otherwise polar density profile, we find by a straightforward integration the estimate $\eta_M = R_{\text{TF}}\sqrt{1 - (1 - M)^{2/5}}$, where R_{TF} is the Thomas-Fermi radius [23].

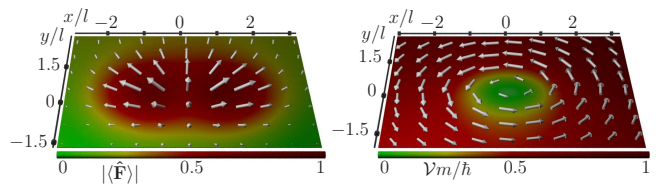


FIG. 1. Left: Spin profile $\langle \hat{\mathbf{F}} \rangle$ (arrows, whose length and color gradient give $|\langle \hat{\mathbf{F}} \rangle|$) of the energetically stable coreless vortex in the polar regime, interpolating between FM and polar phases and displaying the characteristic fountain texture inside the core of a singular polar vortex. Right: The corresponding continuously varying superfluid velocity \mathbf{v} and its magnitude (arrows), and circulation density $\mathcal{V} = \rho\mathbf{v} \cdot \hat{\varphi}$ (color gradient) [23].

As the energy of the imprinted coreless vortex relaxes, the outer region approaches the singly quantized vortex with $F \rightarrow 0$. In the limit of weak magnetization, the vortex core splits into two half-quantum vortices, similarly to the splitting of a singly quantized vortex when magnetization is not conserved [21]. At $M = 0$, the fountain texture is lost entirely. When M increases, the stable coreless-vortex spin texture gradually becomes more pronounced, preventing the core splitting. The vortex (Fig. 1) still maintains the axial asymmetry of the magnetized core region with two close-lying spin maxima $F = 1$, and $\langle \hat{\mathbf{F}} \rangle \parallel \hat{z}$ at the center. Ignoring the slight core asymmetry, the vortex can be qualitatively described by the analytic model (3): The spin winds to $\langle \hat{\mathbf{F}} \rangle \parallel \hat{\rho}$ as ρ increases. Simultaneously, F decreases sharply and the configuration approaches a singly quantized polar vortex. The size of the core (the magnetization density half width at half maximum) is $\sim \eta_M$. Comparison of length scales then suggests that the coreless texture becomes pronounced when $\eta_M \gtrsim \xi_F$ ($> \xi_n$), in qualitative agreement with our numerics.

Owing to the trap, F can reach a local minimum—which may not vanish in all directions—and start increasing at the edge of the cloud. The vortex profile then depends on M and, e.g., on the quadratic Zeeman shift that favors the polar phase [62]. We may therefore envisage a scheme to engineer the core symmetry and even more complex composite defects by Laguerre-Gaussian lasers that generate a Zeeman shift with a cylindrical shell symmetry.

For stronger magnetization we obtain an effective two-component coreless-vortex state, where ζ_0 represents a singly quantized vortex whose core is filled by ζ_+ . The transition to the two-component system occurs when the $\beta(\rho)$ profile no longer allows the three-component vortex (3) to satisfy the magnetization constraint, depopulating ζ_- . The threshold magnetization value decreases with rotation until at $\Omega \simeq 0.35\omega$ the coreless vortex is stable only in the two-component regime (Fig. 2). For

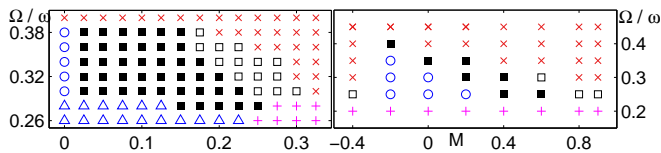


FIG. 2. Stability of the coreless vortex in the polar (left) and FM (right) interaction regimes; (■) stable coreless vortex; (□) stable effective two-component coreless vortex; (△) instability towards a half-quantum vortex, (○) pair of half-quantum vortices (polar regime) or singular vortex (FM regime), (+) vortex-free state; (×) nucleation of additional vortices;

large c_0 , the stable two-component solution represents a smooth transition from the $F = 1$ coreless vortex at the trap center to the $F = 0$ singular vortex at the edge of the cloud.

Next we study the stability of the coreless vortex with conserved magnetization in the FM regime using $Nc_0 = 1000\hbar\omega l^3$ and $Nc_2 \simeq -5\hbar\omega l^3$ of ^{87}Rb [63]. In this case the FM phase with $F = 1$ is preserved everywhere in the imprinted spinor ζ^i during relaxation. We find that imposed weak magnetization can lead to energetic instability of the coreless vortex, with a singular vortex then becoming the rotating ground state. This may seem surprising, since when the magnetization is not conserved in energy relaxation, coreless vortices are predicted to form the ground state at sufficiently rapid rotation [8–11, 21]; a singular vortex may then also be energetically (meta)stable, but always has a higher energy than the coreless vortex [21].

If magnetization is not conserved, its value for the stable coreless spin texture at the trap center is sensitive to rotation, e.g., varying in the studied case from $M \simeq 0.56$ at $\Omega \simeq 0.25\omega$ to $M \simeq 0.34$ at $\Omega \simeq 0.3\omega$. When the conservation of magnetization imposes weaker magnetization at a given rotation frequency, we find that the vortex is displaced from the trap center as it adjusts to the constraint. At very weak M the coreless vortex is forced close to the edge of the cloud and splits into a pair of singular vortices, one of which exits the BEC. At faster rotation, the fountain profile bends more sharply, and consequently a smaller M can be conserved in the coreless-vortex ground state (Fig. 2) [64].

The magnetic-field rotation technique used to phase-imprint the FM coreless vortex [15, 16] can also be applied to a BEC prepared in the polar state $\zeta^0 = (0, 1, 0)^T$ [16, 17], in which the nematic axis $\hat{\mathbf{d}} = \hat{\mathbf{z}}$ and $M = 0$. The rotation $\zeta^p = \exp[-i\hat{\mathbf{F}} \cdot \beta'(\rho)\hat{\boldsymbol{\varphi}}]\zeta^0$ [16] induced by the magnetic-field sweep then leads to the nematic texture $\hat{\mathbf{d}} = \sin\beta'\hat{\boldsymbol{\rho}} + \cos\beta'\hat{\mathbf{z}}$, which defines a *nematic coreless vortex*. Owing to the magnetic field rotation, this always exhibits vanishing longitudinal magnetization. In Ref. [17] an ATC-like (MH-like) texture was imprinted, with $\beta'(\rho = 0) = 0$ and $\beta' = \pi$ ($\beta' = \pi/2$)

at the edge of the cloud. The winding number W may be defined by taking $\hat{\mathbf{n}}_F \rightarrow \hat{\mathbf{d}}$ in Eq. (4). The value of $\hat{\mathbf{d}}$ is not fixed at the boundary, and the coreless nematic texture may smoothly dissolve. Unlike the spin texture of the ordinary coreless vortex, it cannot be stabilized by rotation, due to its vanishing mass circulation.

We ask instead whether the nematic coreless vortex can be stable inside the core of a composite topological defect when a conserved, nonzero magnetization necessitates formation of nonpolar regions. A nematic coreless vortex with a nonzero magnetization could be created by phase-imprinting via population transfer [44, 65, 66] that individually prepares the appropriate phase windings of $\langle -2\pi, 0, +2\pi \rangle$ in the spinor components. In order to describe the composite core structure of the nematic coreless vortex we introduce the spinor wave function

$$\zeta^n = \frac{1}{2} \begin{pmatrix} \sqrt{2}e^{-i\varphi} \left(f_+ \cos^2 \frac{\beta}{2} - f_- \sin^2 \frac{\beta}{2} \right) \\ (f_+ + f_-) \sin \beta \\ \sqrt{2}e^{i\varphi} \left(f_+ \sin^2 \frac{\beta}{2} - f_- \cos^2 \frac{\beta}{2} \right) \end{pmatrix}, \quad (5)$$

where $\langle \hat{\mathbf{F}} \rangle = F(\sin\beta\hat{\boldsymbol{\rho}} + \cos\beta\hat{\mathbf{z}})$. From $\hat{\mathbf{d}} \perp \langle \hat{\mathbf{F}} \rangle$, it follows that in order to have the fountain texture in $\hat{\mathbf{d}}$ we must have $\beta = \pi/2$ at $\rho = 0$ and increasing monotonically. Then when $F(\rho)$ increases with ρ from $F = 0$ to $F = 1$, ζ^n interpolates smoothly from the interior nematic coreless vortex to an outer singular FM vortex with radial spin component $\langle \hat{\mathbf{F}} \rangle_\rho = \sin\beta$, with $\beta \simeq \pi$ at the edge of the cloud (MH-like texture). The corresponding mass circulation, $\oint d\mathbf{r} \cdot \mathbf{v} = -\frac{\hbar F}{m} \cos\beta$, interpolates from the noncirculating polar core to a nonzero circulation, in principle, allowing stabilization by rotation [23].

We find that the numerical relaxation process of the phase-imprinted $\langle -2\pi, 0, +2\pi \rangle$ vortex configuration at given magnetization M can be qualitatively described by the spinor (5). The energetic stabilization of the nematic coreless vortex, however, requires a negative magnetization $M \lesssim -0.2$, strong enough that ζ_+ is depopulated. The polar phase is then realized only where ζ_0 fills the vortex line in ζ_- , with the fountain structure in $\hat{\mathbf{d}}$ [23]. The core size is again determined by the magnetization constraint [23]. The instability at weaker magnetization results from the existence of lower-energy singular vortices with FM cores.

In conclusion, we have shown that the conservation of magnetization in spinor BECs makes it possible to produce vortex core structures with distinct small and large-distance topology. The characteristic core size is then determined by the magnetization constraint, instead of one of the healing lengths associated with the nonlinear interactions. In phase-imprinting experiments of coreless vortices, the magnetization of the initial vortex state can be controlled and the relaxation process of appropriately prepared initial states results in mixing of the different ground-state manifolds. In particular, a nonsingular,

coreless vortex with sufficiently strong magnetization is energetically stable in the polar regime where simple energetic arguments alone would not predict its existence. We have also shown that the stable configuration can be qualitatively understood by an analytic model for the spinor wave function that interpolates between the FM and polar phases, representing a composite topological defect.

We acknowledge financial support from the Leverhulme Trust and EPSRC.

Supplemental Material

In this Supplemental online material we provide additional information regarding spin-1 mean-field theory, conservation of magnetization, phase imprinting of non-singular vortices, and construction of analytic spinor wave functions for the coreless textures.

HAMILTONIAN DENSITY, MAGNETIZATION AND LENGTH SCALES

Hamiltonian density: We treat the spin-1 Bose-Einstein condensate (BEC) in the Gross-Pitaevskii mean-field theory. The Hamiltonian density then reads [5, 6]

$$\mathcal{H} = \frac{\hbar^2}{2m} |\nabla\Psi|^2 + \frac{1}{2}m\omega^2 r^2 n + \frac{c_0}{2}n^2 + \frac{c_2}{2}n^2 |\langle \hat{\mathbf{F}} \rangle|^2 + g_1 n \langle \mathbf{B} \cdot \hat{\mathbf{F}} \rangle + g_2 n \langle (\mathbf{B} \cdot \hat{\mathbf{F}})^2 \rangle, \quad (\text{S1})$$

where $n = \Psi^\dagger \Psi$ is the atom density and m is the atomic mass. We have assumed an isotropic, harmonic trap of frequency ω . The condensate wave function Ψ is now a three-component spinor,

$$\Psi(\mathbf{r}) = \sqrt{n(\mathbf{r})} \zeta(\mathbf{r}) = \sqrt{n(\mathbf{r})} \begin{pmatrix} \zeta_+(\mathbf{r}) \\ \zeta_0(\mathbf{r}) \\ \zeta_-(\mathbf{r}) \end{pmatrix}, \quad \zeta^\dagger \zeta = 1, \quad (\text{S2})$$

in the basis of spin projection onto the z axis. The local condensate spin is the expectation value $\langle \hat{\mathbf{F}} \rangle = \zeta_\alpha^\dagger \hat{\mathbf{F}}_{\alpha\beta} \zeta_\beta$ of the spin operator $\hat{\mathbf{F}}$, defined as a vector of spin-1 Pauli matrices. Linear and quadratic Zeeman shifts, of strength g_1 and g_2 respectively, described by the last two terms of Eq. (S1), may arise from a weak external magnetic field \mathbf{B} .

Spin-independent and spin-dependent interaction terms with strengths $c_0 = 4\pi\hbar^2(2a_2 + a_0)/3m$ and $c_2 = 4\pi\hbar^2(a_2 - a_0)/3m$, respectively, arise from the two scattering channels of colliding spin-1 atoms with s -wave scattering lengths a_0 and a_2 . Minimization of the interaction energy then leads to the two distinct phases of the spin-1 BEC: $c_2 < 0$ favors the $|\langle \hat{\mathbf{F}} \rangle| = 1$ ferromagnetic (FM) phase (e.g., in ^{87}Rb), while the $|\langle \hat{\mathbf{F}} \rangle| = 0$ polar phase is favored when $c_2 > 0$ (e.g., in ^{23}Na).

Conservation of magnetization: We find stable vortex structures by minimizing the free energy $E = \int d^3r \mathcal{H} - \Omega \langle \hat{L}_z \rangle$ in the frame rotating at frequency Ω about the z axis, using imaginary-time propagation of the coupled Gross-Pitaevskii equations. However, the only spin-flip processes possible in s -wave scattering are $2|m=0\rangle \rightleftharpoons |m=+1\rangle + |m=-1\rangle$. Therefore s -wave interaction does not change the *longitudinal magnetization*

$$M = \frac{N_+ - N_-}{N} = \frac{1}{N} \int d^3r n(\mathbf{r}) F_z(\mathbf{r}), \quad (\text{S3})$$

where N is the total number of atoms, N_\pm are the populations of the $|m = \pm 1\rangle$ levels and F_z is the z component of the spin vector. Consequently, M is approximately conserved on time scales where s -wave scattering dominates over, e.g., dipolar interactions and collisions with high-temperature atoms. This is the relevant time scale in present experiments with spinor BECs of alkali-metal atoms [12–14]. We take this conservation strictly into account throughout energy relaxation.

Characteristic length scales: The interaction terms in Eq. (S1) give rise to the characteristic density and spin healing lengths,

$$\xi_n = l \left(\frac{\hbar\omega}{2c_0 n} \right)^{1/2}, \quad \xi_F = l \left(\frac{\hbar\omega}{2|c_2|n} \right)^{1/2}, \quad (\text{S4})$$

where we have introduced the oscillator length $l = (\hbar/m\omega)^{1/2}$ of the harmonic confinement. The healing lengths determine, respectively, the length scales over which the atomic density $n(\mathbf{r})$ and the spin magnitude $|\langle \hat{\mathbf{F}} \rangle|$ heal around a local perturbation. When magnetization is not conserved, ξ_n and ξ_F determine the core size of singular defects [20, 21]. If ξ_F is sufficiently larger than ξ_n , it becomes energetically favorable to avoid depleting the atomic density, instead accommodating the singularity by exciting the wave function out of its ground-state manifold. The core then expands to the order of ξ_F , instead of the smaller ξ_n that determines the size of a core with vanishing density. The lower gradient energy in the larger core offsets the cost in interaction energy.

Conservation of magnetization introduces a third length scale η_M , which is the size required for a magnetized vortex core in an otherwise unmagnetized condensate to give rise to a given magnetization (S3). Here we specifically study a coreless vortex that is phase-imprinted in the polar BEC. As the energy of the coreless vortex relaxes, the core region remains magnetized, but the spin magnitude sharply decreases outside the core. In order to estimate the magnetization length scale we represent the magnetized core by a cylinder of radius η_M , with $\langle \hat{\mathbf{F}} \rangle = \hat{\mathbf{z}}$ everywhere inside, and $|\langle \hat{\mathbf{F}} \rangle| = 0$ outside. The total magnetization is then

$$M(\eta_M) = \frac{1}{N} \int d^3r \Theta(\eta_M - \rho) n_{\text{TF}}(\mathbf{r}), \quad (\text{S5})$$

where $\rho = (x^2 + y^2)^{1/2}$ and Θ is the Heaviside function. We approximate the atomic-density profile by the Thomas-Fermi solution

$$n_{\text{TF}}(r) = \frac{15N}{8\pi R_{\text{TF}}^3} \left(1 - \frac{r^2}{R_{\text{TF}}^2}\right), \quad r \leq R_{\text{TF}}, \quad (\text{S6})$$

where $r = (\rho^2 + z^2)^{1/2}$, and

$$R_{\text{TF}} = l \left(\frac{15 N c_{\text{p,f}}}{4\pi \hbar \omega l^3} \right)^{1/5} \quad (\text{S7})$$

is the Thomas-Fermi radius. Here $c_{\text{p}} = c_0$ in a BEC with polar interactions, and $c_{\text{f}} = c_0 + c_2$ in the FM regime. Computing the integral in Eq. (S5) and solving for η_M as a function of M , we obtain

$$\eta_M = R_{\text{TF}} \sqrt{1 - (1 - M)^{2/5}}. \quad (\text{S8})$$

We also consider a nonsingular coreless vortex formed by a nematic axis. This was experimentally phase imprinted in a polar BEC in Refs. [16, 17]. If the imprinted vortex state carries a finite magnetization (S3), the relaxation of the structure may be described by a spinor wave function that interpolates between the polar and FM phases, so that the core forms a composite topological defect where the interior represents the polar phase. We can then define a length scale η_M^* that describes the size of the polar core at a given magnetization. We estimate η_M^* by taking $\langle \hat{\mathbf{F}} \rangle = \hat{\mathbf{z}}$ everywhere outside a cylindrical core of this radius, and again approximating the density profile by the Thomas-Fermi solution. Then the magnetization is

$$M(\eta_M^*) = \frac{1}{N} \int d^3r \Theta(\rho - \eta_M^*) n_{\text{TF}}(\mathbf{r}). \quad (\text{S9})$$

Solving for η_M^* yields

$$\eta_M^* = R_{\text{TF}} \sqrt{1 - M^{2/5}}. \quad (\text{S10})$$

PHASE IMPRINTING OF NONSINGULAR VORTICES

Two different methods have been demonstrated for controlled preparation of nonsingular vortices. Here we give a brief overview of each.

In Refs. [15, 16] a coreless vortex was prepared using a time-dependent magnetic field to induce spin rotations. This technique was first proposed theoretically in Ref. [56] and was also implemented experimentally to prepare singly and doubly quantized vortices in a spin-polarized BEC [57, 58].

The creation of a coreless vortex in the spin-1 BEC begins with a condensate prepared in a fully spin-polarized

state, which we take to be $\zeta^1 = (1, 0, 0)^T$ [67]. The condensate is subject to an external three-dimensional magnetic quadrupole field [16]

$$\mathbf{B} = B' \rho \hat{\rho} + [B_z(t) - 2B'z] \hat{\mathbf{z}}, \quad (\text{S11})$$

where we have introduced cylindrical coordinates (ρ, φ, z) . The zero-field point $z = B_z/2B'$ ($\rho = 0$) of the quadrupole field is initially at large z so that $\mathbf{B} \parallel \hat{\mathbf{z}}$ in the condensate.

The coreless-vortex structure is created by linearly sweeping $B_z(t)$ so that the zero-field point passes through the condensate. The changing B_z causes the magnetic field away from the z axis to rotate around $\hat{\varphi}$ from the $\hat{\mathbf{z}}$ to the $-\hat{\mathbf{z}}$ direction. The rate of change of the magnetic field decreases with the distance ρ from the symmetry axis. Where the rate of change is sufficiently slow, the atomic spins adiabatically follow the magnetic field, corresponding to a complete transfer from ζ_+ to ζ_- in the laboratory frame. However, where the rate of change of the magnetic field is rapid, atomic spin rotation is no longer adiabatic. In the laboratory frame, the spins thus rotate through an angle $\beta(\rho)$, given by the local adiabaticity of the magnetic-field sweep, which increases monotonically from zero on the symmetry axis. Linearly ramping $B_z(t)$ thus directly implements the spin rotation

$$\zeta^i(\mathbf{r}) = e^{-i\hat{\mathbf{F}} \cdot \beta(\rho) \hat{\varphi}} \zeta^1 = \frac{1}{\sqrt{2}} \begin{pmatrix} \sqrt{2} \cos^2 \frac{\beta}{2} \\ e^{i\varphi} \sin \beta \\ \sqrt{2} e^{2i\varphi} \sin^2 \frac{\beta}{2} \end{pmatrix}. \quad (\text{S12})$$

The resulting fountainlike spin texture

$$\langle \hat{\mathbf{F}} \rangle = \sin \beta \hat{\rho} + \cos \beta \hat{\mathbf{z}} \quad (\text{S13})$$

that defines the coreless vortex in the spinor BEC is analogous to the Anderson-Toulouse-Chechetkin (ATC) [1, 2] and Mermin-Ho (MH) [3] vortices that arise in the A phase of superfluid liquid ^3He . In liquid ^3He , a circulation-carrying, nonsingular, fountainlike texture is formed by the local angular-momentum vector \mathbf{l} of the Cooper pairs. In the ATC texture, \mathbf{l} winds by π from the $\hat{\mathbf{z}}$ direction at the center to the $-\hat{\mathbf{z}}$ direction at the edge of the vortex, while the MH texture exhibits a $\pi/2$ rotation.

The first controlled preparation of a nonsingular vortex [15] used a two-dimensional quadrupole field together with an axial bias field. The magnetic field in the trap is then $\mathbf{B}(\rho, \varphi, \theta) = B_z(t) \hat{\mathbf{z}} + B' \rho [\cos(2\varphi) \hat{\rho} - \sin(2\varphi) \hat{\varphi}]$. By the mechanism described above, ramping of $B_z(t)$ then causes a spin rotation $\zeta(\mathbf{r}) = \exp[-i\hat{\mathbf{F}} \cdot \beta(\rho) \hat{\mathbf{n}}] \zeta^1$ about an axis $\hat{\mathbf{n}}(\varphi) = \sin \varphi \hat{\mathbf{x}} + \cos \varphi \hat{\mathbf{y}}$. The rotation yields a nonsingular spin texture exhibiting a cross disgyration, instead of the fountainlike structure. The two are topologically equivalent.

Another technique for phase imprinting a coreless vortex was recently demonstrated in Ref. [44]. In this experiment, the coreless vortex was created in the $|m = \pm 2\rangle$

and $|m=0\rangle$ magnetic sublevels of the spin-2 manifold of ^{87}Rb . The phase imprinting starts with a spin-polarized condensate in the $|m=+2\rangle$ level, with a magnetic field along the z axis. Collinear σ^- and σ^+ polarized laser beams along the symmetry axis then couple $|m=2\rangle$ to the $|m=0\rangle$ and $|m=-2\rangle$ levels. The laser beams have Laguerre-Gaussian (LG) and Gaussian intensity profiles, respectively, so that the population transferred to the $|m=0\rangle$ ($|m=-2\rangle$) level pick up a 2π (4π) phase winding. The intensity minimum of the LG beam leaves a remaining population in $|m=2\rangle$ with no phase winding. The resulting five-component spinor represents a coreless vortex with the spin structure (S13) when the three nonempty levels of the five-component spinor are regarded as a (pseudo)spin-1 system. The bending angle β is determined by the density profiles of the nonempty spinor components. The laser beams inducing the Raman coupling of the magnetic sublevels can be tailored with a high degree of control, and the vortex structure can therefore be precisely engineered.

By accurately creating specific spin textures, phase imprinting of coreless vortices gives control over the longitudinal magnetization of the cloud, regardless of whether interactions are polar or FM. In the spin-2 coreless-vortex experiment [44], the resulting magnetization in the spin-2 manifold is measured at $M = 0.64$ for an imprinted ATC-like spin texture, and at $M = 0.72$ for a MH-like texture. In the magnetic-field rotation experiment [15] the local magnetization $\mathcal{M}(\mathbf{r}) = [n_+(\mathbf{r}) - n_-(\mathbf{r})]/n(\mathbf{r})$ is reported to be ~ 0.7 at the center of the cloud and ~ -0.5 at the edge. Because of the lower density in the negatively magnetized region, also this vortex can be estimated to carry a positive, nonzero magnetization M .

GENERALIZED VORTEX SOLUTIONS

Coreless vortex

The two phases of the spin-1 BEC have different order-parameter symmetries that support different topological defects. For an overview, see, e.g., Refs. [5, 43]. Here we are interested in nonsingular coreless vortex states that mix the two phases. In order to construct spinor wave functions representing such vortices, we consider first a representative spinor with uniform spin $\langle \hat{\mathbf{F}} \rangle = F \hat{\mathbf{z}}$:

$$\zeta^F = \frac{1}{\sqrt{2}} \begin{pmatrix} -\sqrt{1+F} \\ 0 \\ \sqrt{1-F} \end{pmatrix}. \quad (\text{S14})$$

In particular, the limits $F = 0$ and $F = 1$ yield $\zeta^F|_{F=0} = (-1/\sqrt{2}, 0, 1/\sqrt{2})^T$ and $\zeta^F|_{F=1} = (-1, 0, 0)^T$, respectively, corresponding to representative polar and FM spinors. Any other spinor with $|\langle \hat{\mathbf{F}} \rangle| = F$ can be reached by applying a condensate phase ϕ

and a three-dimensional spin rotation $U(\alpha, \beta, \gamma) = \exp(-i\hat{\mathbf{F}}_z\alpha)\exp(-i\hat{\mathbf{F}}_y\beta)\exp(-i\hat{\mathbf{F}}_z\gamma)$, defined by three Euler angles, to Eq. (S14). We may thus write the most general spinor as

$$\zeta = \frac{e^{i\phi}}{2} \begin{pmatrix} \sqrt{2}e^{-i\alpha} \left(e^{i\gamma} f_- \sin^2 \frac{\beta}{2} - e^{-i\gamma} f_+ \cos^2 \frac{\beta}{2} \right) \\ - (e^{i\gamma} f_- + e^{-i\gamma} f_+) \sin \beta \\ \sqrt{2}e^{i\alpha} \left(e^{i\gamma} f_- \cos^2 \frac{\beta}{2} - e^{-i\gamma} f_+ \sin^2 \frac{\beta}{2} \right) \end{pmatrix}, \quad (\text{S15})$$

where $f_{\pm} = \sqrt{1 \pm F}$.

The state (S15) can also be specified by the condensate phase, the spin magnitude F and an orthonormal triad with one vector in the direction of the spin. One of the remaining vectors in the triad forms the nematic axis $\hat{\mathbf{d}}$. (In the polar limit, $\hat{\mathbf{d}}$ fully specifies the state together with the condensate phase [20].) In the representative spinor (S14) we choose the triad such that $\hat{\mathbf{d}} = \hat{\mathbf{x}}$. In the general spinor (S15), $\hat{\mathbf{d}}$ can then be found from the Euler angles.

By allowing $\phi, \alpha, \beta, \gamma$ and the spin magnitude F to vary in space, we can now construct generalized solutions representing the coreless vortex states in a condensate where FM and polar regions coexist and the wave function interpolates smoothly between them. In Eq. (S15) we choose $\phi = \alpha = \varphi$ (where φ is the azimuthal angle) and $\gamma = 0$ to yield [Eq. (3) of the main text]:

$$\zeta^{\text{cl}}(\mathbf{r}) = \frac{1}{2} \begin{pmatrix} \sqrt{2} \left(f_- \sin^2 \frac{\beta}{2} - f_+ \cos^2 \frac{\beta}{2} \right) \\ -e^{i\varphi} (f_- + f_+) \sin \beta \\ \sqrt{2}e^{2i\varphi} \left(f_- \cos^2 \frac{\beta}{2} - f_+ \sin^2 \frac{\beta}{2} \right) \end{pmatrix}. \quad (\text{S16})$$

The spin texture is then given by

$$\langle \hat{\mathbf{F}} \rangle = F(\mathbf{r})[\sin \beta(\mathbf{r})\hat{\boldsymbol{\rho}} + \cos \beta(\mathbf{r})\hat{\mathbf{z}}], \quad (\text{S17})$$

where $\beta(\mathbf{r})$ increases monotonically from zero on the symmetry axis to form the characteristic fountain texture with varying spin magnitude $F(\mathbf{r})$. In the limit $F = 1$, we retrieve the coreless vortex represented by Eqs. (S12) and (S13). In the polar limit $F = 0$, on the other hand, Eq. (S16) represents a singly quantized vortex

$$\zeta^{\text{cl}}|_{F \rightarrow 0} = \frac{e^{i\varphi}}{\sqrt{2}} \begin{pmatrix} -e^{-i\varphi} \cos \beta \\ -\sqrt{2} \sin \beta \\ e^{i\varphi} \cos \beta \end{pmatrix}, \quad (\text{S18})$$

where we have explicitly separated out the condensate phase $\phi = \varphi$. The nematic axis forms the texture $\hat{\mathbf{d}} = \cos \beta \hat{\boldsymbol{\rho}} - \sin \beta \hat{\mathbf{z}}$. In general the spin rotation that accompanies the winding of the condensate phase therefore represents a disgyration of the nematic axis.

The vortex (S16) can represent a solution for which F is nonuniform, so that Eqs. (S12) and (S18) are the two limiting solutions. We can form a composite topological defect by setting $F(\rho = 0) = 1$ and $\beta(\rho = 0) = 0$ at the center and letting $F \rightarrow 0$ and $\beta \rightarrow \pi/2$ as ρ increases.

Then the core exhibits a coreless-vortex fountain texture that continuously transforms toward a singular polar vortex as the radius increases.

The mixing of the polar and FM phases in the vortex configuration is also reflected in the superfluid circulation. From Eq. (S15) we derive the general expression

$$\mathbf{v} = \frac{\hbar}{m} \nabla \phi - \frac{\hbar F}{m} [\nabla \gamma + (\nabla \alpha) \cos \beta]. \quad (\text{S19})$$

for the superfluid velocity \mathbf{v} . For the coreless vortex (S16) this reduces to

$$\mathbf{v}^{\text{cl}} = \frac{\hbar}{m\rho} [1 - F(\rho) \cos \beta(\rho)] \hat{\boldsymbol{\varphi}}, \quad (\text{S20})$$

when F and β depend only on the radial distance ρ . By considering a circular loop \mathcal{C} at constant ρ enclosing the vortex line, we can then compute the circulation

$$\nu = \int_{\mathcal{C}} d\mathbf{r} \cdot \mathbf{v}^{\text{cl}} = \frac{\hbar}{m} [1 - F(\rho) \cos \beta(\rho)], \quad (\text{S21})$$

We may regard the integrand of Eq. (S21) as a *circulation density*

$$\mathcal{V}(\mathbf{r}) = \mathbf{v}(\mathbf{r}) \cdot \hat{\boldsymbol{\varphi}}\rho, \quad (\text{S22})$$

along a cylindrically symmetric path. The circulation of Eq. (S16) continuously interpolates between the polar and FM phases, smoothly connecting the small-distance and large-distance topology of the vortex. Note that it further follows from Eq. (S19) that circulation alone is quantized only in the limit $F \rightarrow 0$.

Owing to the effectively two-dimensional structure of the coreless spin texture, it is possible to define a winding number

$$W = \frac{1}{8\pi} \int_{\mathcal{S}} d\Omega_i \epsilon_{ijk} \hat{\mathbf{n}}_F \cdot \left(\frac{\partial \hat{\mathbf{n}}_F}{\partial x_j} \times \frac{\partial \hat{\mathbf{n}}_F}{\partial x_k} \right). \quad (\text{S23})$$

Here the integral is evaluated over the upper hemisphere \mathcal{S} , and $\hat{\mathbf{n}}_F = \langle \hat{\mathbf{F}} \rangle / |\langle \hat{\mathbf{F}} \rangle|$ is a unit vector in the direction of the local spin vector. The charge W defines a topological invariant if the boundary condition on $\hat{\mathbf{n}}_F$ away from the vortex is fixed. When the asymptotic texture is uniform, W is an integer (representing a mapping between the spin texture and a compactified two-dimensional plane).

In the coreless vortex in the spinor BEC, asymptotic behavior of the spin texture is determined by rotation, as the bending of β in Eq. (S16), and therefore the circulation (S21), adapts to minimize the energy. The spin texture away from the vortex line may also be determined by interactions with other vortices, e.g., in the formation of a composite defect. By substituting $\langle \hat{\mathbf{F}} \rangle$ from Eq. (S17) into Eq. (S23), we may evaluate W . Assuming cylindrical symmetry and taking R to be the radial extent of the spin texture, we find

$$W = \frac{1 - \cos \beta(R)}{2}, \quad (\text{S24})$$

where we have used $\beta = 0$ on the z axis, such that $\hat{\mathbf{n}}_F|_{\rho=0} = \hat{\mathbf{z}}$. The winding number now depends on the asymptotic value of $\beta(\rho)$, such that for $\beta(R) = \pi$ (ATC-like texture) $W = 1$, and for $\beta(R) = \pi/2$ (MH-like texture) $W = 1/2$.

Nematic coreless vortex

From Eq. (S15) we can also construct the spinor for a *nematic coreless vortex* in a magnetized polar BEC. In this case we note that we wish to construct a vortex where

$$\hat{\mathbf{d}} = \sin \beta' \hat{\boldsymbol{\rho}} + \cos \beta' \hat{\mathbf{z}}, \quad (\text{S25})$$

corresponding to the state phase-imprinted by Choi et al. [16, 17]. The angle β' between $\hat{\mathbf{d}}$ and the z axis increases from $\beta' = 0$ at $\rho = 0$ to $\beta' = \pi/2$ ($\beta' = \pi$) at the edge for a MH-like (ATC-like) texture. Note that since the Euler angles in Eq. (S15) represent spin rotations of Eq. (S14), we have $\beta = \beta' + \pi/2$, such that $\beta = \pi/2$ at the center of the vortex. The desired vortex state can then be constructed by additionally choosing $\alpha = \varphi$, $\gamma = \pi$ and $\phi = 0$ to yield [Eq. (5) of the main text]

$$\zeta^n = \frac{1}{2} \begin{pmatrix} \sqrt{2} e^{-i\varphi} \left(f_+ \cos^2 \frac{\beta}{2} - f_- \sin^2 \frac{\beta}{2} \right) \\ (f_+ + f_-) \sin \beta \\ \sqrt{2} e^{i\varphi} \left(f_+ \sin^2 \frac{\beta}{2} - f_- \cos^2 \frac{\beta}{2} \right) \end{pmatrix}, \quad (\text{S26})$$

with spin profile $\langle \hat{\mathbf{F}} \rangle = F(\sin \beta \hat{\boldsymbol{\rho}} + \cos \beta \hat{\mathbf{z}})$.

In a magnetized BEC, Eq. (S26) can represent a composite vortex that mixes the FM and polar phases. We consider a solution for which F exhibits a spatial structure interpolating between $F \rightarrow 0$ at the center and $F \rightarrow 1$ at the edge of the cloud. In the limit $F \rightarrow 1$, Eq. (S26) becomes a singular singly quantized FM vortex,

$$\zeta^n|_{F \rightarrow 1} = \frac{1}{\sqrt{2}} \begin{pmatrix} \sqrt{2} e^{-i\varphi} \cos^2 \frac{\beta}{2} \\ \sin \beta \\ \sqrt{2} e^{i\varphi} \sin^2 \frac{\beta}{2} \end{pmatrix}. \quad (\text{S27})$$

We calculate the superfluid circulation by assuming F and β in Eq. (S26) to be functions of the radial distance ρ only,

$$\mathbf{v}^n = -\frac{\hbar F}{m\rho} \cos \beta \hat{\boldsymbol{\varphi}}. \quad (\text{S28})$$

Similarly, we find the circulation density $\mathcal{V}(\mathbf{r}) = -\hbar F(\rho) \cos \beta(\rho)/m$ and circulation

$$\nu = \int_{\mathcal{C}} d\mathbf{r} \cdot \mathbf{v}^n = -\frac{\hbar F}{m} \cos \beta, \quad (\text{S29})$$

assuming a circular path \mathcal{C} at constant ρ . It follows that circulation vanishes for the nematic coreless vortex in the

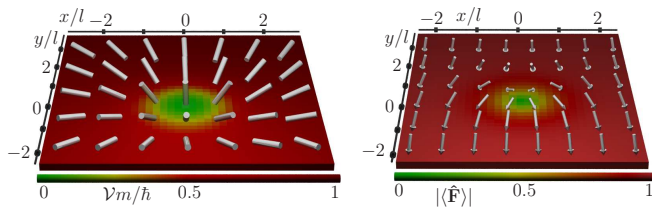


FIG. S1. Stable coreless nematic vortex in a BEC with polar interactions. Left: The unoriented $\hat{\mathbf{d}}$ -vector (cylinders) exhibits the coreless fountainlike texture. The circulation density $\mathcal{V} = \rho \mathbf{v} \cdot \hat{\boldsymbol{\varphi}}$ (color gradient) shows the composite-vortex structure that interpolates between the noncirculating polar phase to the outer singly quantized FM vortex. Right: Corresponding spin texture $\langle \hat{\mathbf{F}} \rangle$ (arrows) and spin magnitude $|\langle \hat{\mathbf{F}} \rangle|$ (color gradient and arrow lengths), showing the core region. Conservation of magnetization forces the BEC into the FM phase away from the vortex line.

pure polar phase $F \rightarrow 0$ and becomes nonzero for $F > 0$ ($\cos \beta \neq 0$).

The interpolation between the polar and FM regimes is illustrated in the numerically computed, stable nematic coreless vortex in both spin magnitude and circulation density in Fig. S1. The vortex is energetically stable only once magnetization is strong enough to deplete ζ_+ , enforcing an effective two-component regime. The stable vortex exhibits a MH-like texture in $\hat{\mathbf{d}}$, and a corresponding winding of the spin vector from the $\hat{\boldsymbol{\rho}}$ direction at the center to the $-\hat{\mathbf{z}}$ direction in the FM region.

Also for the nematic coreless vortex we may define a winding number analogous to Eq. (S23), associated with the fountain texture of the nematic axis $\hat{\mathbf{d}}$, by taking $\hat{\mathbf{n}}_F = \hat{\mathbf{d}}$. Note that due to the equivalence $\hat{\mathbf{d}} \leftrightarrow -\hat{\mathbf{d}}$ the sign of W is no longer well defined. For the cylindrically symmetric fountain texture (S25), the integral in Eq. (S23) can be evaluated to yield

$$W = \frac{1 - \cos \beta'(R)}{2} = \frac{1 - \sin \beta(R)}{2}, \quad (\text{S30})$$

making use of $\beta' = 0$ on the symmetry axis where $\hat{\mathbf{d}} = \hat{\mathbf{z}}$. In the last step we have used the relation $\beta = \beta' + \pi/2$ to rewrite W in terms of the Euler angle β of Eq. (S26). From Eq. (S30), we find $W = 1$ for an ATC-like texture, and $W = 1/2$ for a MH-like texture such as that stabilized in the effective two-component regime (Fig. S1).

[1] V. R. Chechetkin, Zh. Eksp. Teor. Fiz **71**, 1463 (1976).
 [2] P. W. Anderson and G. Toulouse, Phys. Rev. Lett. **38**, 508 (1977).
 [3] N. D. Mermin and T.-L. Ho, Phys. Rev. Lett. **36**, 594 (1976).
 [4] D.-H. Lee and C. L. Kane, Phys. Rev. Lett. **64**, 1313 (1990).
 [5] Y. Kawaguchi and M. Ueda, Phys. Rep. **520**, 253 (2012).

[6] D. M. Stamper-Kurn and M. Ueda, arXiv:1205.1888 (2012).
 [7] T.-L. Ho, Phys. Rev. Lett. **81**, 742 (1998).
 [8] T. Mizushima, K. Machida, and T. Kita, Phys. Rev. Lett. **89**, 030401 (2002).
 [9] J.-P. Martikainen, A. Collin, and K.-A. Suominen, Phys. Rev. A **66**, 053604 (2002).
 [10] J. W. Reijnders, F. J. M. van Lankvelt, K. Schoutens, and N. Read, Phys. Rev. A **69**, 023612 (2004).
 [11] E. J. Mueller, Phys. Rev. A **69**, 033606 (2004).
 [12] J. Stenger, S. Inouye, D. M. Stamper-Kurn, H. Miesner, A. P. Chikkatur, and W. Ketterle, Nature **396**, 345 (1998).
 [13] M.-S. Chang, C. D. Hamley, M. D. Barrett, J. A. Sauer, K. M. Fortier, W. Zhang, L. You, and M. S. Chapman, Phys. Rev. Lett. **92**, 140403 (2004).
 [14] D. Jacob, L. Shao, V. Corre, T. Zibold, L. De Sarlo, E. Mimoun, J. Dalibard, and F. Gerbier, Phys. Rev. A **86**, 061601 (2012).
 [15] A. E. Leanhardt, Y. Shin, D. Kielpinski, D. E. Pritchard, and W. Ketterle, Phys. Rev. Lett. **90**, 140403 (2003).
 [16] J.-y. Choi, W. J. Kwon, M. Lee, H. Jeong, K. An, and Y.-i. Shin, New J. Phys. **14**, 053013 (2012).
 [17] J.-y. Choi, W. J. Kwon, and Y.-i. Shin, Phys. Rev. Lett. **108**, 035301 (2012).
 [18] Ü. Parts, J. M. Karimäki, J. H. Koivuniemi, M. Krusius, V. M. H. Ruutu, E. V. Thuneberg, and G. E. Volovik, Phys. Rev. Lett. **75**, 3320 (1995).
 [19] M. M. Salomaa and G. E. Volovik, Rev. Mod. Phys. **59**, 533 (1987).
 [20] J. Ruostekoski and J. R. Anglin, Phys. Rev. Lett. **91**, 190402 (2003).
 [21] J. Lovegrove, M. O. Borgh, and J. Ruostekoski, Phys. Rev. A **86**, 013613 (2012).
 [22] S. Kobayashi, Y. Kawaguchi, M. Nitta, and M. Ueda, Phys. Rev. A **86**, 023612 (2012).
 [23] See Supplemental Material for details.
 [24] U. Leonhardt and G. Volovik, JETP Lett. **72**, 46 (2000).
 [25] T. Ohmi and K. Machida, J. Phys. Soc. Jpn **67**, 1822 (1998).
 [26] H. T. C. Stoof, E. Vliegen, and U. Al Khawaja, Phys. Rev. Lett. **87**, 120407 (2001).
 [27] S.-K. Yip, Phys. Rev. Lett. **83**, 4677 (1999).
 [28] T. Isoshima and K. Machida, Phys. Rev. A **66**, 023602 (2002).
 [29] T. Mizushima, K. Machida, and T. Kita, Phys. Rev. A **66**, 053610 (2002).
 [30] C. M. Savage and J. Ruostekoski, Phys. Rev. A **68**, 043604 (2003).
 [31] F. Zhou, Int. J. Mod. Phys. B **17**, 2643 (2003).
 [32] H. Saito, Y. Kawaguchi, and M. Ueda, Phys. Rev. Lett. **96**, 065302 (2006).
 [33] L. Santos and T. Pfau, Phys. Rev. Lett. **96**, 190404 (2006).
 [34] V. Pietilä, M. Möttönen, and S. M. M. Virtanen, Phys. Rev. A **76**, 023610 (2007).
 [35] G. W. Semenoff and F. Zhou, Phys. Rev. Lett. **98**, 100401 (2007).
 [36] R. Barnett, A. Turner, and E. Demler, Phys. Rev. A **76**, 013605 (2007).
 [37] A.-C. Ji, W. M. Liu, J. L. Song, and F. Zhou, Phys. Rev. Lett. **101**, 010402 (2008).
 [38] M. Takahashi, V. Pietilä, M. Möttönen, T. Mizushima,

- and K. Machida, Phys. Rev. A **79**, 023618 (2009).
- [39] J. A. M. Huhtamäki, T. P. Simula, M. Kobayashi, and K. Machida, Phys. Rev. A **80**, 051601 (2009).
- [40] M. Kobayashi, Y. Kawaguchi, M. Nitta, and M. Ueda, Phys. Rev. Lett. **103**, 115301 (2009).
- [41] T. P. Simula, J. A. M. Huhtamäki, M. Takahashi, T. Mizushima, and K. Machida, J. Phys. Soc. Jpn **80**, 013001 (2011).
- [42] M. O. Borgh and J. Ruostekoski, Phys. Rev. Lett. **109**, 015302 (2012).
- [43] M. O. Borgh and J. Ruostekoski, Phys. Rev. A **87**, 033617 (2013).
- [44] L. S. Leslie, A. Hansen, K. C. Wright, B. M. Deutsch, and N. P. Bigelow, Phys. Rev. Lett. **103**, 250401 (2009).
- [45] L. E. Sadler, J. M. Higbie, S. R. Leslie, M. Vengalattore, and D. M. Stamper-Kurn, Nature **443**, 312 (2006).
- [46] M. Vengalattore, S. R. Leslie, J. Guzman, and D. M. Stamper-Kurn, Phys. Rev. Lett. **100**, 170403 (2008).
- [47] J. Kronjäger, C. Becker, P. Soltan-Panahi, K. Bongs, and K. Sengstock, Phys. Rev. Lett. **105**, 090402 (2010).
- [48] E. M. Bookjans, A. Vinit, and C. Raman, Phys. Rev. Lett. **107**, 195306 (2011).
- [49] N. Manton and P. Sutcliffe, *Topological Solitons* (Cambridge University Press, 2004).
- [50] T. H. R. Skyrme, Proc. R. Soc. London A **260**, 127 (1961).
- [51] J. Ruostekoski and J. R. Anglin, Phys. Rev. Lett. **86**, 3934 (2001).
- [52] R. A. Battye, N. R. Cooper, and P. M. Sutcliffe, Phys. Rev. Lett. **88**, 080401 (2002).
- [53] C. M. Savage and J. Ruostekoski, Phys. Rev. Lett. **91**, 010403 (2003).
- [54] J. Ruostekoski, Phys. Rev. A **70**, 041601 (2004).
- [55] T. Kawakami, T. Mizushima, M. Nitta, and K. Machida, Phys. Rev. Lett. **109**, 015301 (2012).
- [56] T. Isoshima, M. Nakahara, T. Ohmi, and K. Machida, Phys. Rev. A **61**, 063610 (2000).
- [57] A. E. Leanhardt, A. Görlitz, A. P. Chikkatur, D. Kielpinski, Y. Shin, D. E. Pritchard, and W. Ketterle, Phys. Rev. Lett. **89**, 190403 (2002).
- [58] Y. Shin, M. Saba, M. Vengalattore, T. A. Pasquini, C. Sanner, A. E. Leanhardt, M. Prentiss, D. E. Pritchard, and W. Ketterle, Phys. Rev. Lett. **93**, 160406 (2004).
- [59] In Ref. [15] a 2D quadrupole field together with an axial bias field was used to create a nonsingular vortex. See also supplemental material for further details.
- [60] H. Mäkelä and K.-A. Suominen, Phys. Rev. A **75**, 033610 (2007).
- [61] S. Knoop, T. Schuster, R. Scelle, A. Trautmann, J. Appmeier, M. K. Oberthaler, E. Tiesinga, and E. Tiemann, Phys. Rev. A **83**, 042704 (2011).
- [62] J. Ruostekoski and Z. Dutton, Phys. Rev. A **76**, 063607 (2007).
- [63] E. G. M. van Kempen, S. J. J. M. F. Kokkelmans, D. J. Heinzen, and B. J. Verhaar, Phys. Rev. Lett. **88**, 093201 (2002).
- [64] In a strongly magnetized condensate, it becomes energetically favorable to empty ζ_- , stabilizing the coreless vortex as an effective two-component vortex.
- [65] M. R. Matthews, B. P. Anderson, P. C. Haljan, D. S. Hall, C. E. Wieman, and E. A. Cornell, Phys. Rev. Lett. **83**, 2498 (1999).
- [66] M. F. Andersen, C. Ryu, P. Cladé, V. Natarajan, A. Vaziri, K. Helmerson, and W. D. Phillips, Phys. Rev. Lett. **97**, 170406 (2006).
- [67] The experiment in Ref. [16] actually starts from $\zeta = (0, 0, 1)^T$ and creates an “upside-down” coreless vortex.